EUROFUSION WPJET1-PR(16) 15036

R Paprok et al.

Particle Tracking Vacuum Approach Estimate of the Effect of Resonant Magnetic Perturbations on Runaway Electrons in JET Experiments

Preprint of Paper to be submitted for publication in
Journal of Plasma Physics

This work has been carried out within the framework of the EUROfusion Consortium and has received funding from the Euratom research and training programme 2014-2018 under grant agreement No 633053. The views and opinions expressed herein do not necessarily reflect those of the European Commission.

Particle Tracking Vacuum Approach Estimate of the Effect of Resonant Magnetic Perturbations on Runaway Electrons in JET Experiments

R.Papřok[1,2], P. Cahyna[1], V.Riccardo[3], J.Mlynář[1], L.Krlín[1], R.Pánek[1] and JET Contributors[*]

1. *Institute of Plasma Physics of the Czech Academy of Sciences, Za Slovankou 1782/3, 182 00 Prague 8, Czech Republic*
2. *Charles University in Prague, Faculty of Mathematics and Physic, Ke Karlovu 3, 121 16 Prague 2, Czech Republic*
3. *EUROfusion Consortium, JET, Culham Science Centre, Abingdon, OX14 3DB, UK*

Abstract

In this paper we present results of simulations of runaway electron trajectories in a JET equilibrium magnetic field under the influence of resonant magnetic perturbations (RMP) created by Error Field Correction Coils. We have studied an influence of magnetic field ripple as well. Motivations for this work was a theoretical support for dedicated runaway electrons suppression experiments during past JET campaigns [1,2]. Results of our particle tracking simulation are in agreement with the negative suppression experimental results. On the other hand, the simulations show possible effectiveness of resonant magnetic perturbation method with twice increased value of the current in perturbation coils compared to maximally available value available in the past experiments.

1. Introduction

It is known from experience that relativistic runaway electrons can be produced during plasma disruptions as well as during operation at low plasma densities or sawtooth instabilities when a significant parallel electric field is induced. Their energy typically reach several units or tenths of MeV unless further increase of their energy is limited by some of another effects [3]. Conversion rate of I_{RE}/I_{plasma} during most dangerous disruptions is usually 50–70 %, under some particular conditions can be up to 80% [4]. ITER and future large tokamaks will be probably even more susceptible to very effective conversion of plasma current to runaway current during plasma disruptions due to avalanche mechanism [5]. Generally, there is a large uncertainty about runaways spatial and energy distribution, which leads to an uncertainty in precise prediction of heat loads on the first wall of tokamak as well. In unfavourable cases they can unfortunately lead to melting and ablation of plasma facing components of the first wall or divertor tiles [6, 7]. Estimates predict that heat load can reach locally ≈ 50 MJ/m2/0.3s what is much more than technically sustainable material limit for transient events like ELMs ≈ 8 MW/m2. It is therefore necessary to develop an effective and

[*] See the Appendix of F. Romanelli et al., Proceedings of the 25th IAEA Fusion Energy Conference 2014, Saint Petersburg, Russia

reliable mitigating mechanism(s) for the runaway electrons suppression before ITER starts to operate around the year 2025. Otherwise it is very probable that influence of runaways will substantially decrease lifetime of ITER plasma facing components and frequent, timely and costly repairs or replacements of these components will be needed.

RE mitigation methods in general

Mitigation methods are based principally on two different phenomena. First type is based on enhanced deconfinement, increased radial transport of runaways due to the destruction of closed nested magnetic surfaces. The fast loss of runaways prohibit further dangerous acceleration. Second type of mitigation methods is based on enhanced collisional drag force due to very fast and substantial increase of particle density of plasma or impurities, usually some noble gases. This abrupt increase of density is 10- to 100-fold compared to the previous plasma density and presents technical challenge in many respects [6, 7]. Method using resonant magnetic perturbations [8,9] belongs to the first class of methods, methods of massive gas injections or (killer) pellets injection usually lead to combination of both principles, because they lead to abrupt increase of density as well as to the destruction of ideal axisymmetric magnetic surfaces.

Runaway electrons RMP experiments and related theoretical works

The onset of runaways avalanche [5] could be suppressed if the runaways were lost from the plasma at a sufficiently high rate. One mechanism capable to cause such a diffusion of runaways out of the plasma volume are magnetic perturbations [10]. When the trajectories become chaotic they once hit the wall and so cannot induce further secondary runaways and subsequent avalanching is suppressed. The RMP mitigation method was firstly experimentally tested on JT-60U [9] and was proposed as a solution for ITER in [6]. On TEXTOR, Dynamic Ergodic Divertor (DED) was used to generate the magnetic perturbations and it was again shown that the RMP were able to suppress runaway electrons generation [11]. It was also shown by means of numerical simulation that trajectories indeed become chaotic in the DED field. Similar type of simulations for the case of planned ITER RMP coils were published in papers [12a, 12b, 12c].

JET RE suppression experiments and motivation of our simulations

The reliability of the resonant magnetic perturbation suppression technique was tested on JET as well with the help of the perturbation field created by the Error Field Correction Coils (EFCCs). While initial results were uncertain [1], it was then found that this had been caused only by the scatter in the data and further dedicated set of experiments have not shown any impact of the EFCCs on runaway electrons [2].

Another type of magnetic perturbation naturally present in the tokamaks is the toroidal field ripple caused by the finite number of toroidal field coils. JET tokamak has unique ability of controlling the ripple as its 32 toroidal field coils are divided into two independently powered sets of 16 coils alternating in the toroidal direction. The smallest ripple is produced when the same current is used in both windings and it increases with an increasing difference between winding currents. Runaway electrons control was experimentally

attempted using the ripple introduced by this way. Theoretical arguments show, that runaways trajectories can be influenced by the ripple [13]. The experiments shown negative suppression effect, i.e. no effect on runaway electrons was observed [2].

In order to, at least partially, explain JET results, we have performed simulations of runaways trajectories in the field of the JET EFCC and in the magnetic field with the ripple. Runaways were modelled as single test particles moving in the background magnetic field, without interactions with other particles. Resulting total magnetic field was obtained as an ideal superposition of the axisymmetric magnetic field and the perturbation magnetic field caused by externally applied field from EFCC. While this 'vacuum approach' would be questionable for simulations of influence of magnetic perturbations used e.g. to control Edge Localized Modes due to the important plasma response and very long magnetic field penetration times (>1s), for the case of post-disruption runaways it is not supposed to be a big problem. After a thermal quench the plasma resistivity is much higher than in flat top phase. Moreover, we can assume that the plasma rotation and gradients are lower than in the flat top phase due to various disruption effects. So externally applied magnetic field penetrates post-disruption plasma quite fast. Calculating the typical penetration time quantitatively from the magnetic diffusion equation and Spitzer resistivity, it is on a time scale of approximatively 1ms or even less.

2. Runaway electrons equations of motion used in simulations

We used in our simulations drift equations derived in [14] for a non-relativistic case and extended in [15] for the relativistic case. The relativistic case, which is necessary for the simulations of the runaway electrons, is based on the Hamiltonian in the normalized form

$$H = \left[\epsilon_0^2 + \epsilon_0\left(p_x^2 + \frac{(p_\phi - f_\phi)^2}{(1+x)^2} + (p_z - f_z)^2\right)\right]^{1/2} + \Phi \qquad (1)$$

where $\varepsilon_0 = c^2/(\omega_c R_0)^2$ is electrons normalized rest energy ($\omega_c = eB_0/m_0c$), $x = (R-R_0)/R_0$ is proportional to radial coordinate, p_x, p_Φ and p_z are normalized momenta and f_z and f_Φ are normalized components of magnetic vector potential assuming $f_x=0$ for the unperturbed magnetic field background (this choice is always possible due to the gauge invariance of magnetic vector potential). Φ is in our simulations unused electric potential. This 'full' Hamiltonian and the corresponding canonical equations were used for cross-check of implementation the drift motion.

The drift Hamiltonian itself has the form

$$H = \omega_x I_x + \frac{1}{2}\left[\frac{\left(p_\phi - f_\phi(x_{gc})\right)^2}{\left(1+x_{gc}\right)^2} - \frac{\left(p_t - \Phi(x_{gc})\right)^2}{\epsilon_0} + \epsilon_0\right] \qquad (2)$$

where x_{gc} is guiding-center radial position and I_x, p_z, p_Φ and p_t are canonical momenta, assuming $f_z = -Z_q \ln(1 + x)$ in equation (1) which corresponds to an ideal dependency $\sim B_0R_0/R$ of the toroidal magnetic field. $Z_q = -1$ for electrons. The poloidal magnetic field and

the influence of perturbation are incorporated in p_Φ component of vector potential. For a detailed derivation of the equations and a deeper mathematical description of this guiding center approach see reference [15].

The correctness of the use of the drift approach is based on the important assumption of smallness of RE Larmor radius compared to a size of magnetic structures where a motion is being performed. The Larmor radius of runaway electrons R_g is in the relativistic case given by the following formula

$$R_g = \gamma \frac{m_0 v_{perp}}{qB} \qquad (3)$$

where γ is well-known Lorenz gamma factor, m_0 is the electron rest mass, v_{perp} is the velocity perpendicular to the magnetic field line, q is the elementary charge and B is the magnetic field amplitude. For the JET typical scenario, where the typical magnetic field is ~3T, the total runaway electron energy is in the range from units to tenths of MeV, the ratio of perpendicular to total energy is a low units of tenths, the typical size of runaway electron Larmor radius is ~1cm. Thus the important assumption above is reasonably well satisfied for the exact computation of the particle motion in the axisymmetric magnetic field with nested flux surfaces of JET machine scales ~1-3 m and to a less extent for a precise calculation of motion inside magnetic islands with characteristic lengths of units to tenths of centimeters.

The same Hamiltonian had been used by the TEXTOR team in [11]. We however did not use the mapping approach used in this paper to avoid its complexity and we instead integrated the equations of motion of the gyrocenter using the standard integration scheme. For numerical solution we have used 4^{th} order Runge-Kutta integrator with adaptive time step. Accuracy of our numerical implementation was checked by a set of checks, namely by a) a comparison with full orbit Hamiltonian equations which are of course numerically much slower, b) total energy conservation and c) a comparison of a trapped particle banana orbit width with the analytical calculation in [16].

The simulations for the case with the ripple field were done using only the full Hamiltonian, as the drift Hamiltonian (2) relies on a toroidally symmetric toroidal field, so it cannot be applied in this situation. The maximal time step in this simulation was enforced to be significantly smaller than the Larmor period, approximately 10 times, in order to represent accurately the full gyration motion dynamics.

It should be emphasized that these equations reduce full 6-dimensional phase-space dynamics into a 4-dimensional space unlike more common cases which are 5-dimensional. There exists a variety of other sets of relativistic drift and guiding center equations [e.g. 17 and references therein; 12b].

3. Magnetic fields used in simulations

We used vacuum approach meaning that the total magnetic field used in our simulations

is a superposition consisting of several parts, namely a) the toroidal field, b) the poloidal field and c) the RMP field. The resulting field is taken as a simple superposition, i.e. we do not take into account plasma response and subsequent possible perturbation screening or amplification. As was mentioned above in the text, the toroidal magnetic field is supposed to have an ideal ~1/R dependence in order to not overcomplicate the calculations.

The second part b), background axisymmetric poloidal magnetic field is obtained by the EFIT reconstructions for different plasma current and safety factor profiles corresponding to one pre-disruption time, taken just before the thermal quench (*blue line* in Figure 1) and two post-disruption types of collapsing plasma during the current quench. The poloidal field is one of the main sources of uncertainty in our simulations. The EFIT code, being mainly intended for a reconstruction of the plasma equilibrium, has some limitation during a moment of disruption, e.g. we are in a very fast transient period so we are at the limits of the validity of the Grad-Shafranov equation, we do not have perfectly an axisymmetric plasma (3D effects are relevant here and depend on the kind of the disruption), the induced currents in tokamak vessel play a significant role in the reconstruction etc. Moreover, it needs an assumption on the plasma current profile, which is not well known during a disruption. Because of this reason, two different current profiles were chosen: a) one fairly flat, with a parabolic radial dependency of current density (*red line*), b) another with a centrally peaked current density (*black line*). The a) case corresponds to one extremal case when the post-disruption current is diffused out/flattened as is usual in normal disruption, the case b) imitates the situation where the most of the plasma current is being carried by the runaway electron beam and what is based on experimental observation of central peaking of SXR emission caused by bremsstrahlung and synchrotron radiation. The differences in the current profiles manifest themselves in the resulting profiles of the safety factor q, see Figure 1.

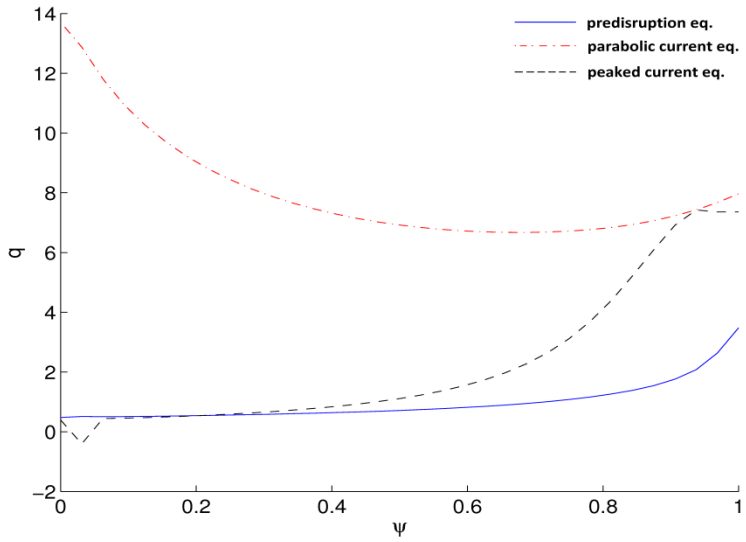

Figure 1: Three different q-profiles used in simulations. One pre-disruption (blue line) low flat q profile and two post-disruption high q flat current profile (red line) and low q peaked current profile (black dashed line).

The last part of the magnetic field represents the influence of JET's Error Field Correction Coils (EFCC). These coils are made from a set of four identical current loops placed around the toroidal direction on the low field side. In our simulations we have considered three cases with different EFCC coil current polarities: a) n=1 with coil currents ++-- toroidally, b) n=1 with polarizations +0-0 and c) n=2 with polarizations +-+-. These polarizations were powered by several current amplitudes, namely 20.8 kAt, 32 kAt, 48 kAt and 96 kAt. All of the current polarities and coil currents up to experimentally available 48kAt amplitude were used in the JET experiments without runaway electron suppression. The experimentally unreachable coil current 96 kAt was used to test whether there is any observable change in the structure of runaway electrons trajectories. The EFCC vector potential was calculated by the ERGOS code [18], which had been previously used for the cases of DIII-D, JET and MAST and proposed design of the ITER RMP coils.

In the last studied case we took into account the presence of non-zero toroidal field ripple. JET has 32 toroidal field coils, thus the usual ripple levels are low (The TF ripple amplitude $\delta(R,Z)=[B_{max}(R,Z) - B_{min}(R,Z)]/[B_{max}(R,Z)+B_{min}(R,Z)]$ is $\delta = 0.08\%$). However, the ripple can be artificially increased by reducing the current carried in every second coil. Ripple values were enhanced up to 1.2%. The JET n=16 toroidal field was calculated by the Biot-Savart's law from the model of the toroidal coils. Grid values of resulting magnetic field were globally interpolated by "psplines" Fortran library [19] and used for a smooth evaluation of magnetic field in arbitrary point of the space.

4. Results of simulations

In our studies we have considered conditions of the JET shot #75352 equipped with a carbon wall. Amplitude of the toroidal magnetic field was 2.7 T in this shot. We have performed approximately 40 runs for different configurations. The results are presented in the form of Poincaré plots, showing for each of 40 initial conditions 2000 toroidal passages of the electron's guiding centre through a chosen fixed poloidal plane. The initial positions are chosen on the outboard midplane in a range from the magnetic axis outwards, to a position 0.8 m. The energies are in the range of runaways experimentally measured energies in JET disruptions: 5 MeV, 10 MeV and 20 MeV. Poincaré sections of one set of simulations for the EFCC current of 20.8 kAt are shown in Figures 2a-c. We do not show results for other currents because they are very similar to this case. Poincaré plots for the speculative current 96 kAt are in Figure 3. Here we can already observe notable ergodization of runaways trajectories in the plasma edge area.

Finally, we did a simulation with the ripple field, which was produced by a current of 63.6 kA in one set of toroidal field and 31.8 kA in the other, corresponding to a $\delta = 1.2\%$ on outer midplane ripple. The results for the pre-disruption equilibrium are shown in Figure 4. For the other equilibria the results were very similar and are not shown here.

All results of our simulations are for clarity summarized in Table 1 below.

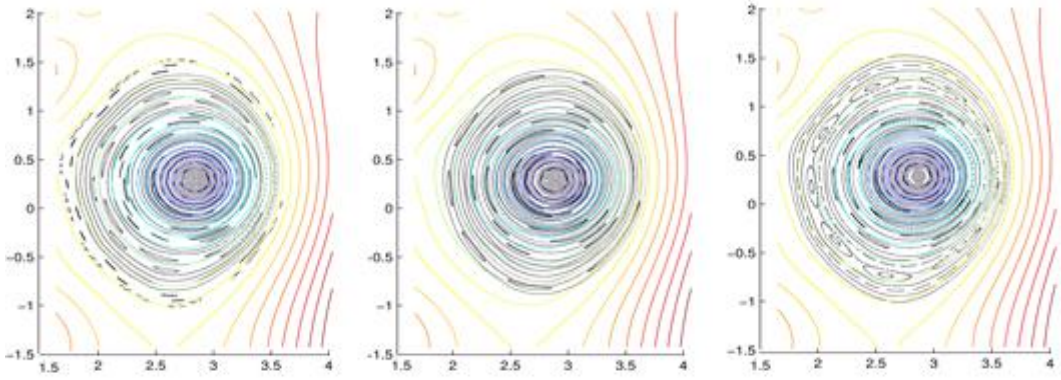

5 MeV 10 MeV 20 MeV

Figure 2a: The case of peaked current profile equilibrium and n=1, +-+- polarizations and 20.8 kAt case (1.3 kA current) for the JET shot #75352. Black dots, usually forming continuous lines, are Poincaré plots of runaways, coloured lines are constant ψ iso-lines.

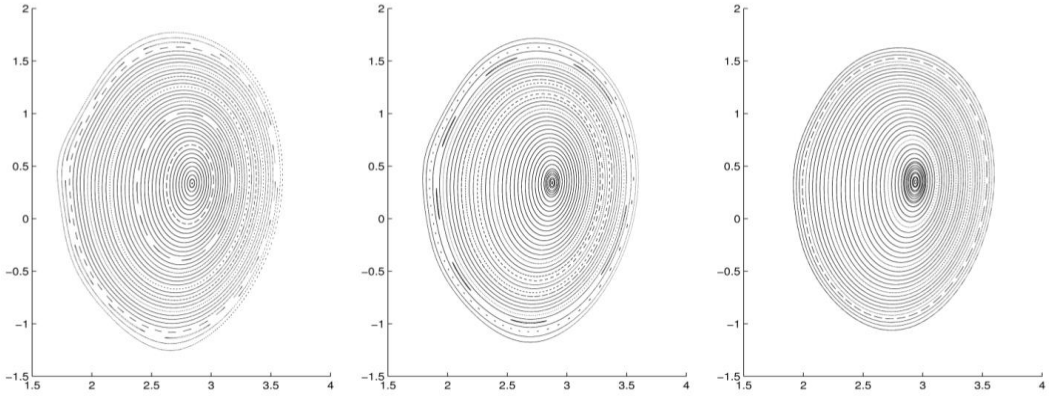

5 MeV 10 MeV 20 MeV

Figure 2b: Poincaré plots for the parabolic current profile equilibrium of the shot #75352, other parameters are same as in Figure 2a.

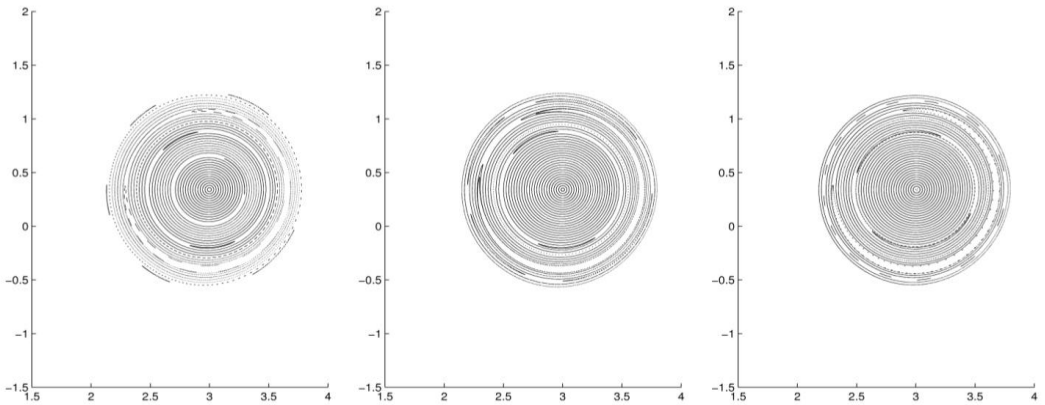

5 MeV 10 MeV 20 MeV

Figure 2c: Poincaré plots for the pre-disruption equilibrium equilibrium of the shot #75352, other parameters are same as in Figure 2a.

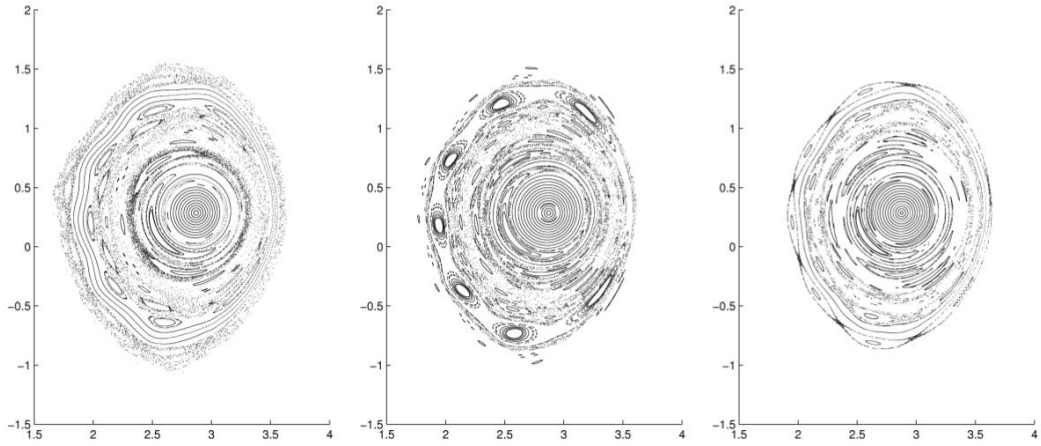

5 MeV 10 MeV 20 MeV

Figure 3: Poincaré plots for the peaked current equilibrium of the JET shot #75352 with n=1 and speculative current 96 kAt (6 kA current) configuration. The case with most pronounced edge ergodization due to the fast of highest simulated perturbation current and a q profile which crosses low resonant surfaces q=1 and q=2 at the plasma edge.

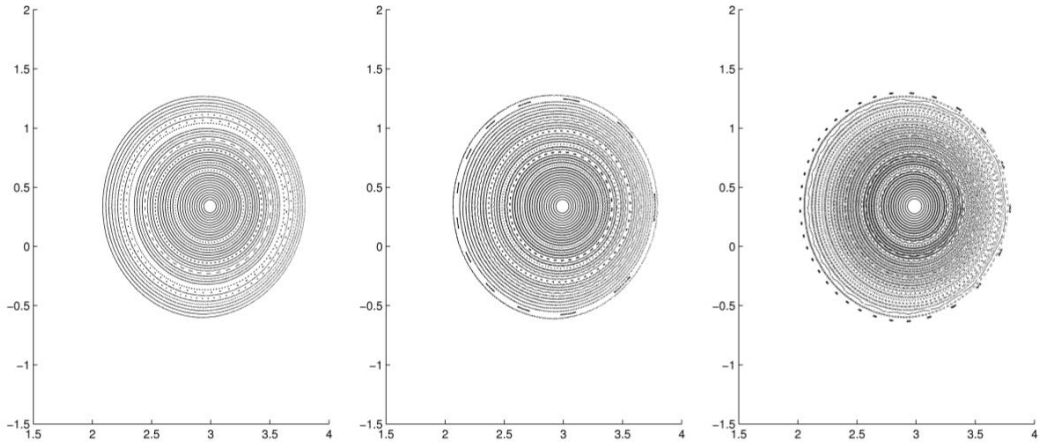

5 MeV 10 MeV 20 MeV

Figure 4: Poincaré plots of runaway trajectories for the toroidal field ripple, pre-disruption equilibrium, JET shot #75352.

Current configuration	Equilibrium	Current (kAt)	E = 5 MeV	E = 10 MeV	E = 20 MeV
n=1, 2 coils	*predisruption*	*32*	regular with islands	regular with islands	regular with islands
	high q/flat j	*32*	regular	regular	regular
	low q/peaked j	*32*	regular with islands	regular with islands	regular with islands

n=1, 4 coils	*predisruption*	*20,8*	regular	regular	regular
	high q/flat j	*20,8*	regular	regular	regular
	low q/peaked j	*20,8*	regular with islands	regular with islands	regular with islands
	predisruption	*96*	chaotic edge	chaotic edge	regular with islands
	high q/flat j	*96*	regular	N/A	N/A
	low q/peaked j	*96*	chaotic edge	chaotic edge	chaotic edge
n=2, 4 coils	*predisruption*	*48*	regular with islands	regular with islands	regular with islands
	high q/flat j	*48*	regular	regular	regular
	low q/peaked j	*48*	regular with islands	regular with islands	regular with islands
	low q/peaked j	*32*	regular with islands	regular with islands	regular with islands

Table 1: *Summary of results of numerical simulations for different EFCC scenarios. Depending on the given scenario, the computed Poincaré belongs to either of the three classes. One exhibits regular dynamics without any presence of X and O points in trajectory phase space, the second class of Poincaré plots contains some islands, but their size is too small to mutually intersect, the third one already contain chaotic sea dynamics, especially in the edge area and is considered to be effective to diffuse out runaways to the wall before they are further dangerously accelerated.*

5. Discussion

All the Poincaré plots show regular Kolmogorov-Arnold-Moser (KAM) surfaces, sometimes alternating with island areas that are too narrow to overlap, except for the case of speculative current 96 kAt. Unfortunately and in agreement with experiment no stochastic transport takes place for experimentally available conditions. The equilibria are however very different. The equilibrium with peaked current profile has the most significant islands because its safety factor passes through the low-order rational numbers. In contrast, for the flat profile equilibrium, the q profile is high so that high poloidal mode numbers m are needed for resonance. Those modes are weak in the spectrum of the EFCCs, because the EFCCs are large coils with a spatially wide perturbation, dominated by low m modes in the Fourier space. The n = 2 perturbation requires for resonances poloidal modes with a twice as high m for the same q profile than the n = 1 perturbation. It is not surprising that the n = 2 results show lesser islands than the n = 1 results. This degree of perturbation would still not be enough to cause runaways losses by itself due to the low Chirikov parameter [2].

Those results explain the experimental observation that runaways are not affected by EFCCs nor the ripple on JET. We tried apparently the most favourable configuration n = 1 with the peaked equilibrium and increased the coil current in the simulation to a speculative value of 96 kAt (6 kA), to see if this would be enough to produce the desired effect (Figure 3). We can see that stochastic regions start to appear, however they do not merge into a global stochastic sea and good KAM surfaces persist especially in the center, where a realistic runaway beam would be located.

On the other hand, runaway electrons transport may be additionally enhanced by other mechanism present in reality but not taken into account in our simulations, such as the

magnetic turbulence [20, 21, 22]. This mechanism has however reduced efficiency for the high runaways energies considered here, because the displacement of drift orbits of the runaways relative to the flux surfaces causes the turbulence, if radially localized, to be averaged out on the runaway orbit [20]. As is shown in reference [21] the influence of electric turbulence is much weaker on highly energetic particles as is the case of high energy runaway electrons, but in energetic region ~10 keV to ~100 keV, what is for JET typical parameters the case of just created runaways, the influence can be important and explain drain of runaway electrons out of the center with very well nested magnetic surfaces. In our simulation we have not included the effect of toroidal electric field acceleration, which can be very high during plasma disruption. The effect of accelerating field was studied for example in [23] and was shown that basic effect of the acceleration by electric field is a shift of the guiding center surface towards the low field side of the tokamak vessel. It represents one important mechanisms which can expel runaway electrons out of the magnetically well confined central plasma region. Soft collisions with background bulk plasma electrons and ions also plays an important role in runaways transport as was shown in [12c].

6. Summary and conclusions

We have shown by our simulations that JET maximal available experimental RMP EFCC coil current (48kAt) was unable to enhance runaway electron transport, due to the inability to sufficiently ergodize runaway electrons dynamics. On the other hand, we can see that under some more favourable circumstances, mainly for the cases with 96kAt coil current (see Figure 3), there is a substantial transport caused by the ergodized magnetic field present and this should have an important impact on runaways transport losses.

Acknowledgement

This work has been carried out within the framework of the EUROfusion Consortium and has received funding from the Euratom research and training programme 2014-2018 under grant agreement #633053. The views and opinions expressed herein do not necessarily reflect those of the European Commission. This work has been also supported by MEYS Project #LM2015045 and #LG14002, and the Czech Science Foundation grant 16-24724S. We also thank David Howell for providing the model of the toroidal coils used to calculated the toroidal field ripple.

References

[1] V. Riccardo, Fusion Science and Technology, Volume 53, Number 4, 2008
[2] V. Riccardo et.al., JET disruption studies in support of ITER, PPCF, Volume 52, Number 12, 2010
[3] H. Knoepfel, D.A. Spong, Runaway electrons in toroidal discharges, NF, Volume 19, Number 6, 1979
[4] J.R. Martin-Solis, B. Esposito, Enhanced Production of Runaway Electrons during a Disruptive Termination of Discharges Heated with Lower Hybrid Power in the Frascati Tokamak Upgrade, Phys. Rev. Lett. 97, 165002, 2006
[5] M.N. Rosenbluth, S.V. Putvinski, Theory for avalanche of runaway electrons in tokamaks, NF, Volume 37, Number 10, 1997

[6] ITER Physics Expert Groups, Chapter 8: Plasma operation and control, NF, Volume 39, Number 12, 1999
[7] T.C. Hender et. al., MHD stability, operational limits and disruptions, NF, Volume 47, Number 6, 2007
[8] K.H. Finken et. al., Influence of the dynamic ergodic divertor on transport properties in TEXTOR, NF, Volume 47, Number 7, 2007
[9] R. Yoshino , S. Tokuda, Runaway electrons in magnetic turbulence and runaway current termination in tokamak discharges, NF, Volume 40, Number 7, 2000
[10] P. Helander, Suppression of runaway electron avalanches by radial diffusion, Phys. Plasmas 7, 4106, 2000
[11] M. Lehnen et. al., Suppression of Runaway Electrons by Resonant Magnetic Perturbations in TEXTOR Disruptions, Phys. Rev. Lett. 100, 255003, 2008
[12a] G. Papp, Runaway electron drift orbits in magnetostatic perturbed fields, NF, Volume 51, Number 4, 2011
[12b] G. Papp, Runaway electron losses caused by resonant magnetic perturbations in ITER , PPCF, 53 095004, 2011
[12c] G. Papp, The effect of resonant magetic perturbations on runaway electron transport in ITER, PPCF 54 125008, 2012
[13] M. Rosenbluth, J.Rax., et al., New ideas in tokamak confinement, 1st Edition, ISBN-13: 978-1563961311, ISBN-10: 1563961318, p. 154, 1994
[14] S.S. Abdullaev, Mapping of drift surfaces in toroidal systems with chaotic magnetic fields, Phys. Plasmas 13, 042509, 2006
[15] A. Wingen, S.S. Abdullaev, Influence of stochastic magnetic fields on relativistic electrons, NF, Volume 46, Number 11, 2006
[16] J. Wesson, Tokamaks, 3rd Edition, p. 126, 2004.
[17] J. Cary, A. Brizard, Hamiltonian theory of guiding-center motion,. Rev. Mod. Phys. 81, 693, 2009
[18] M. Bécoulet, Numerical study of the resonant magnetic perturbations for Type I edge localized modes control in ITER, NF, Volume 48, Number 2, 2008
[19] Doug McCune, PSPLINE - Princeton Spline and Hermite Cubic Interpolation Routines, http://w3.pppl.gov/ntcc/PSPLINE/
[20] I. Entrop et al., Scale Size of Magnetic Turbulence in Tokamaks Probed with 30-MeV Electrons, Phys Rev Lett. 84(16):3606-9, 2000
[21] T. Hauff, F. Jenko, Runaway electron transport via tokamak microturbulence , PoP 16, 102308 , 2009
[22] S.S. Abdullaev, K.H. Finken,M. Forster, New mechanism of runaway electron diffusion due to microturbulence in tokamaks, Phys. Plasmas 19, 072502, 2012
[23] X. Guan et. al., Phase-space dynamics of runaway electrons in tokamaks, Phys. Plasmas 17, 092502, 2010